Journal of Materials Chemistry

Cite this: J. Mater. Chem., 2012, 22, 25409

www.rsc.org/materials

PAPER

Pyrene-directed growth of nanoporous benzimidazole-linked nanofibers and their application to selective CO_2 capture and separation†

Mohammad Gulam Rabbani,[a] Ali Kemal Sekizkardes,[a] Oussama M. El-Kadri,[b] Bilal R. Kaafarani[c] and Hani M. El-Kaderi*[a]

Received 25th July 2012, Accepted 29th October 2012
DOI: 10.1039/c2jm34922a

A pyrene-based benzimidazole-linked polymer (BILP-10) has been synthesized by the co-condensation of 1,3,6,8-tetrakis(4-formylphenyl)pyrene and 1,2,4,5-benzenetetramine tetrahydrochloride in dimethylformamide. The use of pyrene as a molecular building unit leads to the formation of self-assembled nanofibers that have moderate surface area (SA_{BET} = 787 m^2 g^{-1}) and very high CO_2/N_2 (128) and CO_2/CH_4 (18) selectivities at 273 K. Furthermore, results from gas uptake measurements indicate that BILP-10 can store significant amounts of CO_2 (4.0 mmol at 273 K/1.0 bar) and H_2 (1.6 wt% at 77 K/1.0 bar) with respective isosteric heats of adsorption of 38.2 and 9.3 kJ mol^{-1} which exceed all of the previously reported values for BILPs and are among the highest values reported to date for unmodified porous organic polymers. Under high pressure settings, BILP-10 displays moderate uptakes of H_2 (27.3 g L^{-1}, 77 K/40 bar), CH_4 (72 L L^{-1}, 298 K/40 bar), and CO_2 (13.3 mmol g^{-1}, 298 K/40 bar). The unusually high CO_2 and H_2 binding affinities of BILP-10 are presumably facilitated by the amphoteric pore walls of the polymer that contain imidazole moieties and the predominant microporous nature.

1. Introduction

Recent advances in the designed synthesis of porous organic materials have resulted in porous architectures with a broad range of potential applications such as catalysis, sensing, and gas storage and separation.[1–3] Among the attractive features of porous organic networks are exceptionally high surface area, remarkable physiochemical stability, adjustable pore metrics, and chemical nature tunability. The latter property, which is central for selective gas binding and separation, can be accessed through post-synthesis modification processes as in the case of porous polymer networks (PPNs),[4] pre-synthesis functionalization of molecular building units, or by polymerization reactions that introduce chemical heterogeneity into polymers through the formation of heterocyclic building units such as benzimidazole and triazoles or ether- and imine-linkages. To circumvent synthetic challenges like uncontrolled reaction rates or functionalization sites that may take place during post-synthesis modification processes, the use of polymerization protocols that lead to an automatic installation of chemical heterogeneity into the pore walls of porous materials has been instrumental. For example, we have prepared several porous benzimidazole-linked polymers (BILPs) by metal-free co-condensation reactions involving arylaldehyde and *o*-diamine molecular building blocks.[5–7] BILPs display remarkable CO_2 uptake and selectivity over N_2 and CH_4 which make them very promising for future use in CO_2 capture and small gas separation applications.

Porous organic and inorganic–organic hybrid materials have received considerable attention in recent years especially in the area of CO_2 post-combustion capture as a result of their high capacity and moderate binding energy for this greenhouse gas which has been linked to global warming.[3,8] For comparison, the current technology being employed for CO_2 post-combustion capture is based on an amine solution such as aqueous monoethanolamine (MEA) solution (~30 wt%) that chemically binds CO_2 and consumes considerable amounts of energy during regeneration, a required step that significantly reduces the output of coal and natural gas fired plants.[9] In addition to this limitation, amine solutions suffer from other undesirable issues that include chemical decomposition, evaporation and a corrosive nature, making the development of new and improved adsorbent materials essential for mitigating the continuous release of CO_2 to the atmosphere by anthropogenic activity. Of similar concern is CO_2 removal from methane rich gases (natural and landfill

[a]*Department of Chemistry, Virginia Commonwealth University, 1001 W. Main St., Richmond, VA 23284-2006, US. E-mail: helkaderi@vcu.edu; Fax: +1 804 828-8599; Tel: +1 804 828-7505*
[b]*Department of Biology, Chemistry, and Environmental Sciences, American University of Sharjah, PO Box 26666, Sharjah, United Arab Emirates. E-mail: oelkadri@aus.edu; Fax: +971 6 515 2450; Tel: +971 6 515-2787*
[c]*Department of Chemistry, American University of Beirut, Beirut 1107-2020, Lebanon. E-mail: bilal.kaafarani@aub.edu.lb; Fax: +961 1 365217; Tel: +961 3 151451*

† Electronic supplementary information (ESI) available: NMR spectra for monomers, spectral and surface characterization of BILP-10, gas sorption data analysis. See DOI: 10.1039/c2jm34922a

gases) which has been a topical issue because CO_2 reduces the energy density of these gases making their transport, storage and use less efficient.[10] In the U.S. it has been projected that shale gas will constitute 49% of natural gas production in 2035 which corresponds to an increase from 5.0 trillion cubic feet in 2012 to 13.6 trillion cubic feet in 2035 according to the U.S. Energy Information Administration's Annual Energy Outlook for 2012.[11] As such, developing new materials to enhance CO_2/CH_4 separation processes will most likely continue in the near future especially after the advancement of fracturing technologies that lead to a significant increase in shale gas production.

In this study we show that integrating pyrene into the framework of BILPs leads to the formation of self-assembled nanofibers that have one of the highest CO_2 and H_2 binding affinities of unmodified porous organic polymers known to date. Additionally, the same polymer exhibits excellent CO_2 selectivity over CH_4 and N_2. The pyrene units presumably facilitate the formation of nanofiber morphology and growth as a result of their ability to form strong π–π stacking interactions.

2. Experimental section

2.1 Materials and methods

All chemicals were purchased from commercial suppliers (Sigma-Aldrich, Acros Organics, or Frontier Scientific) and used without further purification, unless otherwise noted. 1,3,6,8-Tetrabromopyrene was synthesized using a published procedure.[12] Chromatographic separations were performed using standard flash column chromatography methods using silica gel purchased from Acros Organics (60 Å, 35–70 μm). Elemental microanalyses were performed at the Midwest Microlab, LLC. Solution ^1H and ^{13}C NMR spectra were obtained on a Varian Mercury-300 MHz NMR spectrometer. ^{13}C cross-polarization magic angle spinning (CP-MAS) NMR spectra for solid samples were taken at Spectral Data Services, Inc. Spectra were obtained with samples on a Tecmag-based NMR spectrometer, operating at a H-1 frequency of 363 MHz, using a contact time of 1 ms and a delay of three seconds for the CPMAS experiment; samples were spun at 7.0 kHz. Thermogravimetric analysis (TGA) was carried out using a TA Instruments Q-5000IR series thermal gravimetric analyzer with samples held in 50 μL platinum pans under an atmosphere of air (heating rate 5 °C min^{-1}). For Scanning Electron Microscopy Imaging (SEM), the sample was prepared by dispersing the material onto a sticky carbon surface attached to a flat aluminum sample holder. The sample was then coated with platinum at 1×10^{-5} mbar pressure in a nitrogen atmosphere for 90 seconds before imaging. Images were taken on a Hitachi SU-70 Scanning Electron Microscope. Powder X-ray diffraction data were collected on a Panalytical X'pert pro multipurpose diffractometer (MPD). Samples were mounted on a sample holder and measured using Cu Kα radiation with a 2θ range of 1.5–35. FT-IR spectra were obtained as KBr pellets using a Nicolet-Nexus 670 spectrometer. Porosity and gas sorption experiments were collected using a Quantachrome Autosorb 1-C volumetric analyzer using adsorbates of UHP grade. In a typical experiment, a sample was loaded into a 9 mm large bulb cell (Quantachrome) of known weight and then hooked up to Autosorb 1-C and degassed at 120 °C for 12 h. The degassed sample was refilled with nitrogen, weighed precisely and then transferred back to the analyzer. The temperatures for adsorption measurements were controlled by using a refrigerated bath of liquid nitrogen (77 K), liquid argon (87 K), or a temperature controlled water bath (273 K and 298 K). Hydrogen isotherms were collected at 77 K and 87 K. Carbon dioxide and methane isotherms were collected at 273, 288 and 298 K. Pore Size Distribution (PSD) was calculated using a spherical/cylindrical pore (zeolite) NLDFT adsorption model. High pressure sorption isotherms were run using a VTI HPVA-100 volumetric analyzer. Free space measurements were performed prior to data collection utilizing ultra-high purity helium to establish the appropriate cold zone compensation factors. The skeletal density of the material was determined in the course of analysis for appropriate density correction factorization.

2.2 Synthesis

2.2.1 Synthesis of 1,3,6,8-tetrakis(*p*-formylphenyl)pyrene (TFPPy). A mixture of 1,3,6,8-tetrabromopyrene (1.00 g, 1.93 mmol), 4-formylphenylboronic acid (1.74 g, 11.6 mmol), palladium tetrakis(triphenylphosphine) (0.12 g, 0.10 mmol, 5.2 mol %), and potassium carbonate (2.1 g, 15 mmol) in dry dioxane (30 mL) was stirred under nitrogen for 3 days at 85 °C. The yellow suspension reaction mixture was poured into a solution of ice containing concentrated hydrochloric acid. The yellow solid was filtered, and washed with 2 M HCl (20 mL) three times. The product was extracted with $CHCl_3$ (3 × 100 mL) and dried over $MgSO_4$. After filtration, the solvent was removed under reduced pressure and the resultant solid residue was recrystallized from hot $CHCl_3$ to afford TFPPy as a bright yellow powder (0.85 g, 72%). ^1H NMR (300 MHz, $CDCl_3$, δ): 10.17 (s, 4H, Ar H), 8.18 (s, 4H, Ar H), 8.09 (d, $J = 6$ Hz, 8H, Ar H), 8.05 (s, 2H, Ar H), 7.86 (d, $J = 6$ Hz, 8H, Ar H); UV-vis ($CHCl_3$): $\lambda_{max} = 259$, 290 (sh), 303, 402 nm; IR (KBr): $\nu = 3061$ (w), 2921 (w), 2812 (w), 2721 (w), 1700 (s), 1601 (s), 1566 (w), 1305 (w), 1215 (m), 1169 (m), 1006 (w), 832 (m), 757 (w), 734 (w); MALDI-TOF MS for $C_{44}H_{26}O_4$: $[M]^+$ found 618.11, calcd 618.18. Anal. calcd for $C_{44}H_{26}O_4 \cdot 0.4CHCl_3 \cdot 0.5H_2O$: C 78.95, H 4.05, O 10.66; found: C 78.96, H 4.09, O 10.89%.

2.2.2 Synthesis of BILP-10. A 250 mL Schlenk flask was charged with 1,2,4,5-benzenetetramine tetrahydrochloride (113 mg, 0.39 mmol), 50 mL anhydrous DMF, and a stirrer-bar. The resultant homogeneous solution was cooled to *ca.* −30 °C and treated drop-wise with TFPPy (120 mg, 0.19 mmol) dissolved in anhydrous DMF (115 mL). The temperature was maintained around −30 °C for 6 hours during which a yellowish brown solid formed then the resultant slurry solution was left to warm to room temperature overnight. The flask containing the reaction mixture was flushed with air for 10 minutes and capped tightly. The reaction mixture was then transferred to a static oven and heated gradually to 130 °C (0.5 °C min^{-1}) and kept for 3 days to afford a fluffy yellow powder. The solid was isolated by filtration over a medium glass frit and subsequently washed with DMF, acetone, water, 2 M HCl, 2 M NaOH, water, and acetone. The product was then immersed in acetone–$CHCl_3$ (1 : 1 v/v) for one day, during which time the activation solvent was decanted and freshly replenished twice. After filtration, the product was

dried at 120 °C under vacuum (150 mTorr) to give BILP-10 as a fluffy yellow powder (130 mg, 84%). Anal. calcd for $C_{56}H_{30}N_8 \cdot 8H_2O$: C 70.13, H 4.83, N 11.68; found: C 68.70, H 3.85, N 10.47%.

3. Results and discussion

3.1 Synthesis and characterization of BILP-10

The synthesis of the pyrene-derived BILP-10 was accomplished by using the condensation method we have reported recently for BILPs.[5–7] The proposed mechanism for the formation of the imidazole linkage consists of two steps; the formation of an *in situ* aniline Schiff's base that undergoes subsequent cyclo-dehydrogenation in the presence of molecular oxygen to afford the imidazole ring as illustrated in Scheme 1. This effective and metal-free avenue facilitates the purification processes of the resultant polymers as it eliminates metal ion trapping and leads to the most porous benzimidazole-based polymers. This method also avoids the use of metal catalysts which can be too expensive for the production of CO_2 adsorbents on a large scale.[3]

A schematic representation for the synthesis of BILP-10 is shown in Scheme 2. A homogeneous solution of 1,2,4,5-benzenetetramine tetrahydrochloride (BTA) in dimethylformamide (DMF) was cooled to −30 °C then treated dropwise with 1,3,6,8-tetrakis(4-formylphenyl)pyrene (TFPPy) dissolved in DMF to afford a yellow suspension which is most likely imine-linked networks. The resultant suspension was bubbled with air for 10 minutes then heated for three days at 130 °C to afford BILP-10 as a yellow powder in a good yield (84%). We have noticed previously that the slow addition of aldehyde and the use of low temperatures during the initial polymerization stages were important factors that affect the overall porosity of BILPs.[5] The first step is acid-catalyzed (HCl in this case) even at low temperature (−30 °C) whereas exposure to molecular oxygen and heating over an extended period of time are required for imidazole ring formation.

BILP-10 is insoluble in common organic solvents and was purified by washing with 2 M aqueous solutions of HCl and NaOH, water, and acetone. The chemical composition and connectivity between building units were established using spectral and analytical methods while porosity was investigated by argon sorption–desorption measurements. The chemical connectivity and the formation of the imidazole ring were confirmed by FT-IR and ^{13}C CP-MAS NMR studies.

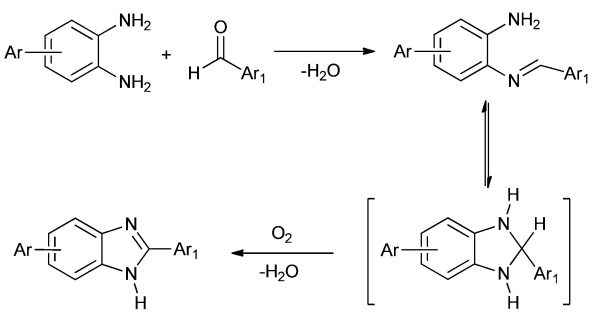

Scheme 1 Proposed mechanism for the formation of imidazole *via* condensation reaction between 1,2-benzenediamine and arylaldehyde.[13]

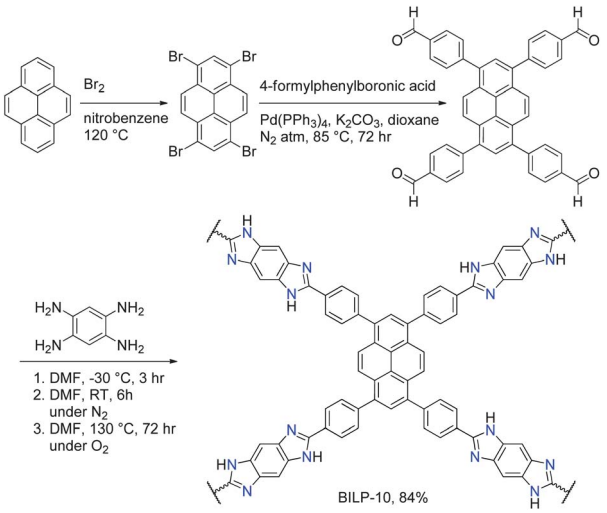

Scheme 2 Synthesis of 1,3,6,8-tetrakis(4-formylphenyl)pyrene and its subsequent use in the preparation of BILP-10 by condensation with 1,2,4,5-benzenetetramine tetrahydrochloride.

The FT-IR spectrum of BILP-10 (Fig. 1A) reveals N–H stretching at around 3412 cm^{-1} (free N–H) and 3205 cm^{-1} (hydrogen bonded N–H), while intense new bands appeared at 1638 cm^{-1} (C=N), and 1484, 1435, 1370 and 1275 cm^{-1} which can be assigned to vibrations of the benzimidazole ring skeleton.[5,14] The intensity of the C=O band at 1700 cm^{-1} in TFPPy is substantially attenuated in BILP-10 which suggested the full consumption of TFPPy monomer during polymerization. The ^{13}C CP-MAS NMR spectrum for BILP-10 (Fig. 1B) contains a signal around 151 ppm that corresponds to NC(Ph)N in the benzimidazole units as well as other signals in the aromatic range that arise from the TFPPy and BTA units.[5–7] The thermal

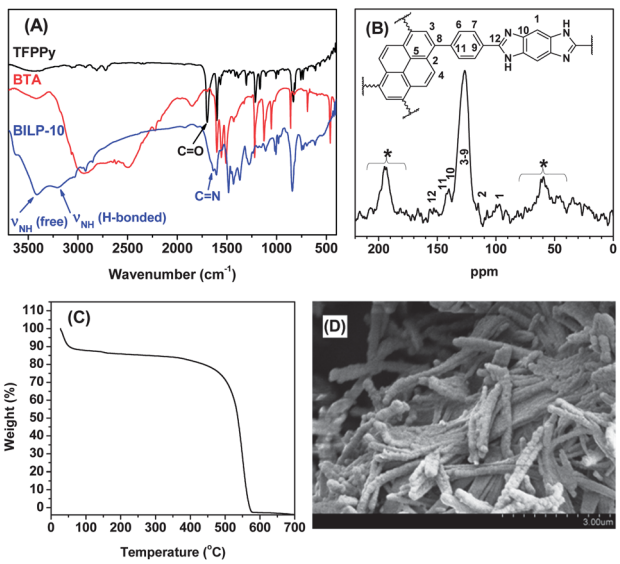

Fig. 1 FT-IR spectra of activated BILP-10, and monomers TFPPy and BTA (A); ^{13}C CP-MAS NMR spectrum of BILP-10 (asterisks denote spinning side bands) (B); thermogravimetric analysis (TGA) of activated BILP-10 (C); and scanning electron microscopy (SEM) image of as-prepared BILP-10 (D).

stability of BILP-10 was confirmed by thermogravimetric analysis (TGA) which indicates that the polymer remains stable up to ~450 °C (Fig. 1C). The material is amorphous as indicated by the powder X-ray diffraction profile of BILP-10 (see ESI,† Fig. S2). Scanning electron microscopy (SEM) revealed a unique morphology of nanofibers of around 0.2 μm in diameter and up to ~7.5 μm in length (Fig. 1D). Worth mentioning is that such directional growth was not observed for the previously reported BILPs. As mentioned above, the nanofiber morphology of BILP-10 is most likely driven by the strong π–π stacking interactions of the rigid and electron-rich pyrene cores. In addition to the π–π stacking interactions, the hydrogen bonding interactions originating from the benzimidazole moieties which are in the same plane as pyrene cores can also facilitate the longitudinal directed self-assemblies of the nanofibers.

3.2 Porosity and gas storage studies

The porosity of BILP-10 was investigated by argon sorption–desorption measurements. The dry polymer was degassed at 140 °C for 12 h to remove any remaining guest molecules before sorption measurements. Fig. 2A shows the argon isotherm for BILP-10 at 87 K. The fully reversible isotherm exhibits a rapid uptake at low pressure (P/P_0 = 0–0.05 bar) followed by a somewhat steep uptake until saturation pressure which indicate the presence of micropores in addition to a minor pore size distribution in the mesoporous range. Applying the Brunauer–Emmett–Teller (BET) model to the sorption branch within the pressure range of P/P_0 = 0.05–0.15 resulted in a specific surface area SA_{BET} = 787 $m^2\ g^{-1}$. Pore size distribution was estimated from the argon isotherm by nonlocal density functional theory (NLDFT) and was found to be centered around 7.6 Å (Fig. 2B), while pore volume (P_{vol} = 0.40 cc g^{-1}) was calculated from a single point measurement at P/P_0 = 0.95. It should be noted that NLDFT investigations also resulted in minor domains of larger pores (10 to 20 Å) which possibly result from a lack of a uniform growth of the polymer's network or solid-state packing. In contrast, calculating the corresponding properties from the nitrogen isotherm leads to a much broader PSD range with pore size ranges centered at about 12.6 Å and 20–50 Å and a cumulative pore volume of 0.457 cc g^{-1} with ~23% contribution from mesopores (see ESI,† Fig. S11). In addition to the subnanometer porosity of BILP-10, altering the chemical heterogeneity of pore walls by introducing nitrogen-rich moieties as in the case of imidazole units has proven to be very important in selective gas uptake and enhanced binding affinities.[5–7] The effectiveness of this approach has been documented for porous materials such as metal–organic frameworks (MOFs) and organic polymers especially for targeted applications directed towards CO_2 storage or separation.[5,8,15] For example, several polymeric systems that contain N-functionalized pore walls, including those of BILPs, that we have reported recently have shown enhanced CO_2 uptakes and selectivity.[3,5] Accordingly, the impact of these factors on the uptake of H_2 and CO_2 and the preferential CO_2 binding over N_2 and CH_4 were investigated. H_2, CO_2, CH_4 gas isotherms were collected and their respective isosteric enthalpies of adsorption (Q_{st}) were calculated. The CO_2 isotherms depicted in Fig. 2C are fully reversible and exhibit a steep rise at low pressures. The absence of adsorption–desorption hysteresis indicates that CO_2 is reversibly adsorbed by BILP-10. The CO_2 uptake (177 mg g^{-1}, 4.0 mmol g^{-1}) at 273 K and 1.0 bar is slightly lower than those of BILPs that have high CO_2 uptakes (188–235 mg g^{-1}), but higher than the values reported for BILPs that were constructed from 2D building units such as BILP-2 and BILP-5 (128–149 mg g^{-1}).[5] To the best of our knowledge, this CO_2 uptake by BILP-10 is among the highest by porous organic polymers such as BILPs (5.3 mmol g^{-1}),[5] carbazole-based porous organic polymers (CPOPs, 4.82 mmol g^{-1})[15] and –OH functionalized porous organic frameworks (POFs, 4.2 mmol g^{-1}),[16] and rivals those of the best performing MOFs under similar experimental settings.[8,9b,17] The CO_2 uptake also exceeds those reported for activated carbon and porous organic materials in general. For example, the uptake of BILP-10 (4.0 mmol g^{-1} at 273 K/1 bar) is higher than those of BPL carbon (3.3 mmol g^{-1}),[18] COFs (1.3–3.8 mmol g^{-1}),[18] functionalized CMPs (1.6–1.8 mmol g^{-1}),[19] porous poly(benzimidazole) PPBIs (1.4–1.8 mmol g^{-1}) and triptycene-based microporous poly(benzimidazole) networks TBIs (2.7–3.9 mmol g^{-1}),[20] triptycene-based cage compounds (2.1 mmol g^{-1})[21] and cucurbit[6]uril (2.9 mmol g^{-1}).[22] BILP-10 also outperforms the best performing ZIFs (ZIF-78, 3.4 mmol g^{-1}).[23]

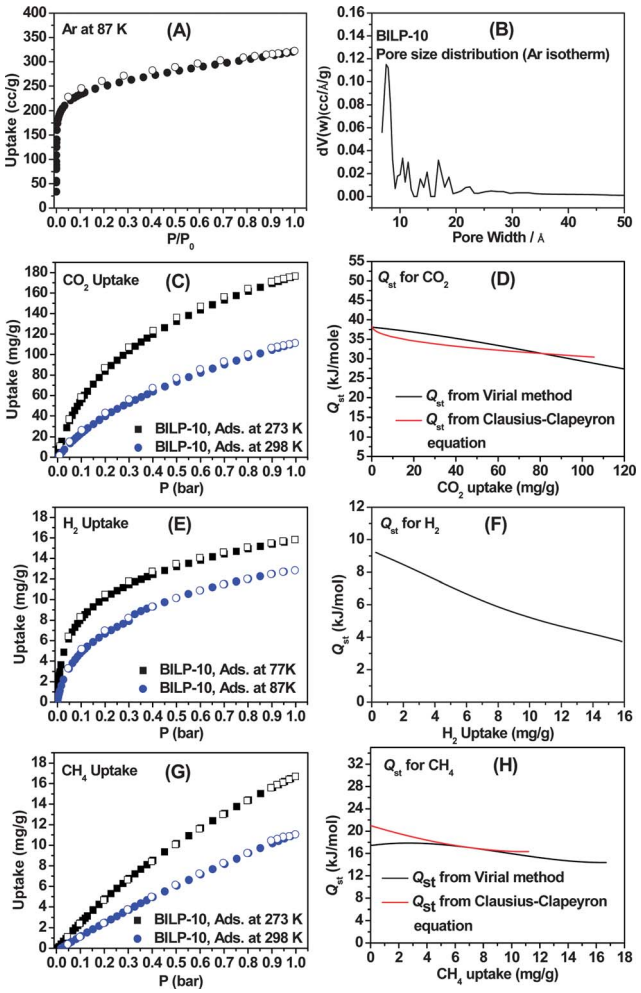

Fig. 2 Argon uptake isotherm (A), PSD from NLDFT (B), CO_2 (C), Q_{st} for CO_2 (D), H_2 (E), Q_{st} for H_2 (F), CH_4 (G), and Q_{st} for CH_4 (H). Adsorption (filled) and desorption (empty).

To determine the binding affinity of BILP-10 for CO_2, we calculated the Q_{st} for CO_2 from the adsorption data collected at 273 and 298 K using the virial method.[24] As shown in Fig. 2D, the Q_{st} value at zero coverage is 38.2 kJ mol^{-1} and drops with higher loading to 22.7 kJ mol^{-1} as the uptake reaches 177 mg g^{-1}. The zero coverage Q_{st} value, to the best of our knowledge, is one of the highest for unmodified purely organic polymers or cage molecules. This value was also confirmed by using the Clausius–Clapeyron equation as overlaid in Fig. 2D.[25]

For the Clausius–Clapeyron equation, CO_2 isotherms at 273, 288 and 298 K were collected and the resulting data were fitted using the Tóth model (see ESI,† Fig. S13). This model has been reported to be superior to the Langmuir or Freundlich models in providing a more extensive data fitting at both low and high surface coverage.[26] The Q_{st} values obtained from the Clausius–Clapeyron equation and the virial method resulted in a very similar trend with increasing surface coverage. As stated above, the CO_2 Q_{st} value is much higher than those of unmodified organic polymers including nitrogen-rich networks PECONFs (26–34)[27] or PI-1 (34)[28] but is lower than CO_2 selective MOFs[9b,17,29] or functionalized PPNs[4] which generally feature –NH_2 or –OH functionalized pores. The high CO_2 uptake and binding affinity of BILP-10 are expected to arise from strong interactions of the polarizable CO_2 molecules through hydrogen bonding and/or dipole–quadrupole interactions that utilize the nitrogen sites of imidazole rings.[9b,30] Other attractive features of BILP-10 are the readily reversible CO_2 sorption–desorption behavior and the moderate Q_{st} value which indicate that CO_2 evacuation from the pores can be performed rapidly and simply by reducing the pressure without heating the polymer. This energy-saving step in post-combustion CO_2 capture is highly desirable because it eliminates energy consumption during adsorbent regeneration as in the case of primary alkanolamines that require significant amounts of heat because of the high heat capacity of water.[9]

Since most BILPs reported thus far show high CO_2 uptakes as a result of their imidazole functionalized pore walls, it is expected that their CO_2 uptake capacity will depend on the number of accessible nitrogen sites that can preferentially bind CO_2. This may be due to the CO_2 interaction with the imidazole moiety through the nitrogen lone-pair of –C=N– and the carbon atom in O=C=O as well as *via* the N–H…O hydrogen bonding interactions (see ESI,† Fig. S18).[31] In order to investigate this factor, a quantitative correlation between the number of available nitrogen adsorption sites *versus* those that would be occupied upon CO_2 adsorption was performed by considering the repeating unit of BILP-10 ($C_{56}H_{30}N_8$). Assuming that each imidazole unit can potentially interact with one CO_2 molecule on average, the calculation predicts that BILP-10 would adsorb 216 mg of CO_2 (*i.e.* 21.6 wt%). Interestingly at 273 K and 1.0 bar, BILP-10 shows an experimental uptake of 177 mg g^{-1} which indicates that ~82% of the available nitrogen centers are associated with CO_2. The remaining vacant nitrogen sites (18%) may not be accessible under the current experimental settings (1.0 bar/273 K) due to the amorphous nature of BILP-10 and its small pores (PSD = 7.6 Å). In addition, the adsorbed CO_2 molecules in narrow pore channels may impede the diffusion of additional CO_2 towards the remaining available nitrogen sites. In order to understand the nature of the adsorbate–adsorbent and adsorbate–adsorbate interactions at different temperatures, the CO_2 isotherms collected at 273 and 298 K were analyzed by virial type eqn (1) (see ESI,† Fig. S19).[32] The less negative value of the first virial coefficient (A_0) at 273 K (−15.31 mol g^{-1} Pa^{-1}) compared to that of 298 K (−16.59 mol g^{-1} Pa^{-1}) suggests stronger CO_2–surface interactions at 273 K. In contrast, the more negative value of the second virial parameter (A_1) at 273 K (−439.54 g mol^{-1}) compared to that of 298 K (−373.52 g mol^{-1}) indicates stronger CO_2–CO_2 interactions inside the pores of the polymer.[32]

The gas storage capacity of BILP-10 was also examined for hydrogen which is a very promising candidate for use in automotive applications due to its abundance and clean aspect.[33] The hydrogen uptake for BILP-10 (1.6 wt%) at 77 K and 1 bar (Fig. 2E) is among the highest values reported for microporous organic polymers.[34] The isotherms are fully reversible and exhibit relatively steep initial uptakes at low pressure which indicate a strong affinity for H_2 gas. The Q_{st} for H_2 was calculated from adsorption data collected at 77 and 87 K (Fig. 2F). At zero-coverage, the Q_{st} value for BILP-10 is 9.3 kJ mol^{-1} which is higher than all values reported recently for BILPs (7.8–8.3 kJ mol^{-1}) and other organic polymers such as polyimide networks (5.3–7.0 kJ mol^{-1}),[35] COFs (3.9–7.0 kJ mol^{-1}),[18] porous aromatic frameworks (PAF-1, 4.6 kJ mol^{-1}),[36] porous polymer networks (PPNs, 5.5–7.6 kJ mol^{-1}),[37] –OH functionalized POFs (8.3 kJ mol^{-1})[16] and tetrazine-based organic frameworks (TzFs, 7.8–8.2 kJ mol^{-1}).[32] Similarly, we recorded CH_4 uptakes at 273 and 298 K up to 1 bar (Fig. 2G) in order to evaluate the potential use of BILP-10 in CO_2/CH_4 separation. Both isotherms are completely reversible and exhibit adsorption maxima of 16.7 and 11.1 mg g^{-1} at 273 and 298 K, respectively. The Q_{st} for CH_4 was calculated by using adsorption data collected at 273 and 298 K using the virial method. At zero coverage, the Q_{st} is 17.5 kJ mol^{-1} (Fig. 2H). The Q_{st} was also calculated using the Clausius–Clapeyron equation by fitting the data collected at 273, 288 and 298 K to the Tóth model and the result was compared to that obtained by the virial method. It was noticeable that the Tóth model gave a slightly higher initial Q_{st} value (20.0 kJ mol^{-1}) however both trends become very similar as the methane loading increases with pressure.

3.3 Gas selectivity studies under equilibrium settings

The gas selectivity of porous materials consisting of pore sizes within the kinetic diameters of small gas molecules solely depends on the difference in affinity of gas components to be adsorbed on the surface of the porous architectures. Selective adsorption and separation of small gas molecules such as CO_2, N_2 and CH_4 have received considerable attention because CO_2 is a major contaminant of natural gas and its release into the atmosphere by anthropogenic activity is a major concern. Given the similar kinetic diameter of these gases, it has been very difficult to develop effective materials for small gas separation that possess the needed physicochemical stability under practical conditions. In order to investigate the potential use of BILP-10 in gas separation applications, isotherms for CO_2, N_2 and CH_4 were collected at 273 and 298 K up to 1.0 bar (Fig. 3).

The initial steep rise in CO_2 compared to N_2 and CH_4 can be attributed to the more favourable interactions between CO_2 and

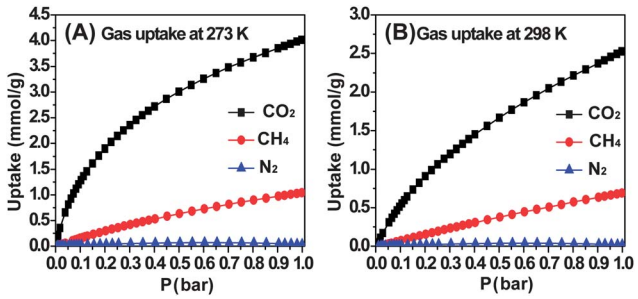

Fig. 3 Gas sorption capacities for BILP-10 at 273 K (A) and 298 K (B). CO_2 (black square), CH_4 (red circle), and N_2 (blue triangle).

the accessible nitrogen sites of imidazole moieties. This preferential and higher affinity of CO_2 compared to N_2 and CH_4 would be very instrumental in CO_2 capture and separation processes. The CO_2/N_2 and CO_2/CH_4 selectivities were calculated from single-component adsorption isotherms using the Henry law constants. These constants can be calculated from the initial slopes of the isotherms in the linear low pressure range ($P < 0.1$ bar).[29b] The selectivities for CO_2/N_2 were found to be 107 (273 K) and 59 (298 K) (see ESI,† Fig. S21). The selectivity value 107 at 273 K is among the highest for reported organic or inorganic-hybrid porous materials that employed the same method for selectivity calculations; for example, BILPs (59–113),[5] PECONF-2 (109),[27] BPL carbon (17.8) and ZIFs (17–50),[23] Bio-MOF-11 (81)[29b] and noncovalent porous materials (NPMs) (74).[38] In addition to this method, recent reports have reported selectivity studies using eqn (1):

$$S = [q_1/q_2]/[p_1/p_2] \quad (1)$$

where S is the selectivity factor, q_i represents the quantity adsorbed of component i, and p_i represents the partial pressure of component i.[8] For post-combustion CO_2 capture, the partial pressure of CO_2 and N_2 are 0.15 bar and 0.75 bar, respectively. According to gas uptakes at these partial pressures, the calculated CO_2/N_2 selectivity values (S) for BILP-10 were found to be 128 (273 K) and 107 (298 K). Interestingly, the latter selectivity is the highest by purely organic materials and only exceeded by $H_3[(Cu_4Cl)_3(BTTri)_8(mmen)_{12}]$ (165).[8] A recent investigation of organic cage molecules has shown that discrete organic molecules can also have high selectivity, however, the high selectivity is compromised by a very modest CO_2 uptake (3.64 cc g^{-1}) at STP[39] which is very low compared to that of BILP-10 (89.3 cc g^{-1}). Although the use of single-component gas isotherms to investigate selectivity has been well documented in recent literature, it should be noted that this approach may not reflect the actual selectivity of the material because this method does not take into consideration the competition between adsorbate molecules for pore binding sites. Nevertheless, this simple method is a convenient, rapid and useful tool to compare the performance of different porous materials in selective adsorption studies.

Following the same procedures described above, we have also studied CO_2/CH_4 selectivity for BILP-10 by collecting isotherms at 273 and 298 K and by subjecting the data to initial slope calculations (see ESI,† Fig. S21). While the CO_2 isotherms exhibit steep uptakes at low pressure, the CH_4 isotherms lead to much lower uptakes (Fig. 3). The CO_2/CH_4 selectivities of BILP-10 were found to be 14 (273 K) and 7 (298 K). These values are similar to those of diimide-based organic polymers,[40] and exceeds reported values for BPL carbon, ZIFs[21] and most MOFs.[10b,41] This selective nature of BILP-10 makes it a promising candidate for use in CO_2 removal from methane-rich gases (natural gas and landfill gas) where CO_2 has to be removed to avoid pipeline corrosion, enhance storage efficiency and increase the heat value. In a typical natural gas purification process, the mole fractions of CO_2 and CH_4 are 0.05 and 0.95, respectively, and the total pressure is maintained at 2 bar, resulting in CO_2 having a partial pressure of only 0.1 bar.[40b] The CO_2/CH_4 selectivity was then calculated according to eqn (1) by using the CO_2 and CH_4 uptakes at 0.1 bar and 1.9 bar, respectively. These calculations resulted in relatively high selectivity levels; $S = 18$ (273 K) and 10 (298 K) that are in good agreement with those obtained from initial slope calculations. Because gas storage and selective uptake can vary at high pressure, we evaluated the performance of BILP-10 in high pressure gas storage and used the resulting isotherms to investigate selectivities of CO_2 over CH_4 and N_2 by the ideal adsorbed solution theory as described below.

3.4 High pressure gas storage studies

For practical use like the onboard storage and use of hydrogen or methane in automotive applications, these gases need to be stored under high pressure conditions in order to meet both volumetric and gravimetric targets. The U.S. Department of Energy (DOE) has set a target for onboard methane storage at 180 v/v at room temperature and 35 bar.[42] While for hydrogen storage, the gravimetric/volumetric system targets for near-ambient temperature (−40 to 85 °C) and moderate pressure (less than 100 bar) are 5.5 wt% and 40 g L^{-1}, respectively, for 2017.[43] Additionally carbon dioxide is usually separated at ambient pressure and then sequestered at a much higher pressure. Given the low density of porous organic polymers, meeting volumetric constraints by organic polymers and other low density materials such as COFs and MOFs has been a considerable challenge especially for methane and hydrogen storage.[3a,10b] Accordingly, high pressure gas isotherms were collected to evaluate the performance of BILP-10 in gas storage under high pressure conditions and the data for gravimetric and volumetric uptakes are presented in Fig. 4.

The gravimetric excess uptake for hydrogen was found to be 3.4 wt% (17.3 mmol g^{-1}) at 77 K/40 bar which is higher than most organic polymers of similar surface area but less than those of high surface area 3D COFs (~7.0 wt%),[18] PAFs (4.2–7.0 wt%),[36] and PPN-4 (8.34 wt%)[4a] collected at a higher pressure (up to 60 bar). The CO_2 uptake was significant at 298 K/40 bar (12.4 mmol g^{-1}) and in the range of reported uptakes for HCPs (10.6–13.3)[44] but falls short of high surface area COFs,[18] PPNs,[4a,37] and PAFs[36] that can reach ~39 mmol g^{-1} at 298 K/55 bar. Similarly, the excess methane uptake at 298 K/40 bar was 4.1 mmol g^{-1} which compares well with values reported for porous organic materials of similar surface areas.[3a] However the storage capacity for methane remains below those of high surface area networks mentioned above. The volumetric storage capacity which determines how densely the gas molecules are stored within the materials is also relevant to express the efficiency of

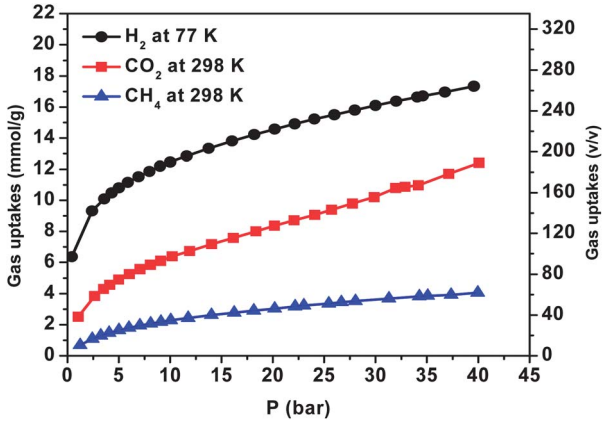

Fig. 4 High pressure surface excess gas sorption uptakes for BILP-10.

adsorbents. The absolute volumetric (v:v) uptake for hydrogen is (303 L L^{-1}) which is comparable to many of the MOFs.[45] Similarly the absolute adsorbed amount for CH_4 in volumetric units was also estimated to be 72 L L^{-1} which is slightly lower than COF-102 (136 L L^{-1}).[18] The volumetric hydrogen and methane uptakes are still short of targets set by the U.S. DOE. The volumetric CO_2 adsorption capacity at 298 K and 35 bar is 175 L L^{-1} which is lower than that of the best performing MOF-177 (320 v/v at 35 bar) but approximately 5 times higher than the quantity stored at this pressure in an empty container.[8]

3.5 High pressure gas selectivity studies

We applied the ideal adsorbed solution theory (IAST)[46] to estimate the selectivity of CO_2 over CH_4 and N_2 as a function of pressure (up to 40 bar) by using the sorption data collected from high pressure gas sorption measurements. The IAST method predicts the adsorption selectivity for gas mixtures based on pure component gas isotherms and has been used to investigate adsorbents such as MOFs,[47] zeolites[48] and organic polymers.[37,40] The predicted CO_2/CH_4 and CO_2/N_2 selectivities for binary gas mixtures of various molar compositions as a function of pressure are shown in Fig. 5. In the very low pressure region, the CO_2/CH_4 selectivity starts to drop rapidly until the pressure reaches ~2 bar and then the selectivity increases steadily. For instance, the selectivity for a gas mixture of CO_2 and CH_4 with a mole fraction ratio of 0.5 : 0.5 (typical feed composition of landfill gas) at 298 K and 0.1 bar is 10.0, which drops to 8.5 at 0.5 bar, then increases to reach 13.7 at 40 bar. The latter value is consistent with that calculated by the initial slope calculation method described above. Most likely at low pressure the nitrogen functional sites of the polymer have much higher binding affinity for CO_2 because of its large quadrupolar moment and with increasing pressure (0 to 2 bar) these sites get saturated and become less available for CO_2 molecules. However, as the pressure increases beyond 2 bar, the selectivity increases due to the higher adsorption potential of CO_2. The observed initial drop in selectivity at low pressures is consistent with the reported trends for diimide-based polymers in the pressure range of 0.1 to 5 bar,[40] while the steady increase of CO_2/CH_4 selectivity upon pressure increase has been reported for PPNs.[37] Notably, the selectivity by BILP-10 at high pressure is more than double those of PPNs. In a

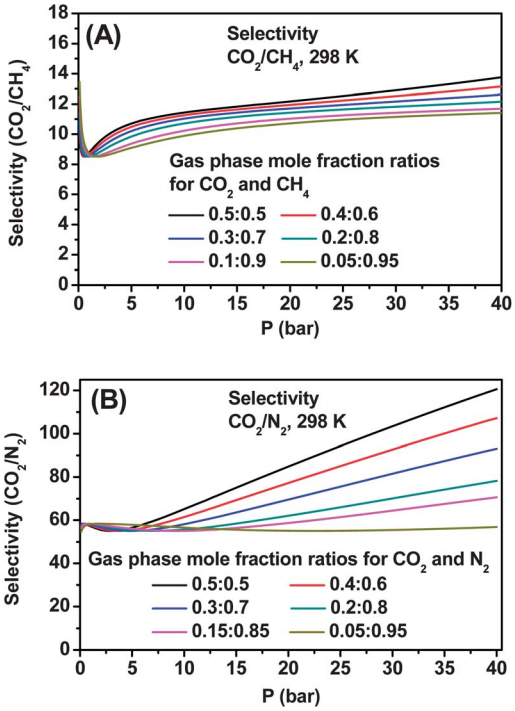

Fig. 5 IAST selectivities of CO_2 over CH_4 (A) and CO_2 over N_2 (B) for binary gas mixtures of variable molar compositions in BILP-10.

similar fashion, we investigated the selectivity of CO_2 over N_2 (Fig. 5B). The overall trend indicates that selectivity increases with pressure and the highest levels were observed for gas mixtures that have high CO_2 compositions. The selectivity approaches 120 and 71 for gas mixtures of 0.5 : 0.5 and 0.15 : 0.85 (typical composition for flue gas from power plants) molar ratios, respectively, at 298 K and 40 bar. At low pressure, IAST predicts the selectivity to be ~57 which agrees very well with that obtained from initial slope calculations (59). Again, the higher selectivity is observed in the high-pressure region for gas mixtures that contain higher CO_2 mole fractions due to the higher adsorption potential of CO_2. The overall results are consistent with the fact that CO_2 is the most strongly adsorbed molecule due to its large quadrupolar moment while methane is more strongly adsorbed than N_2 because of the higher polarizability of CH_4 (26×10^{-25} cm^3) *vs.* N_2 (17.6×10^{-25} cm^3).[49]

4. Conclusions

In conclusion, we have successfully developed a simple synthetic route to incorporate pyrene into the backbone of benzimidazole-linked polymers. The impact of this electron-rich building unit on the solid-state packing of the polymer leads to the formation of a unique nanofiber morphology prompted by the ability of the pyrene units to interact through strong π–π stacking interactions. The formation of such morphology and the predominant microporous nature lead to high CO_2 (18 wt%, 273 K/1.0 bar) and H_2 (1.6 wt% at 77 K/1.0 bar) uptakes. However, BILP-10 stores moderate absolute volumetric amounts of H_2 (27.3 g L^{-1}) and methane (72 L L^{-1}) under high pressure conditions which can limit its use in onboard gas storage applications. While the low pressure gas storage capacities have been exceeded by other

recently reported BILPs; IAST studies indicate that at high pressure, BILP-10 exhibits high selectivity of CO_2 over CH_4 and N_2 which makes BILP-10 a promising material for use in gas separation processes. Additionally, the high isosteric heats of adsorption for H_2 (9.3 kJ mol^{-1}) and CO_2 (38.2 kJ mol^{-1}) observed are among the highest values reported to date for unmodified porous organic polymers or discrete molecules.

Acknowledgements

Research supported by the U.S. Department of Energy, Office of Basic Energy Sciences, Division of Materials Sciences and Engineering under Award number DE-SC0002576. B. R. K. thanks the University Research Board of the American University of Beirut for a Faculty Development Fund. O. M. E.-K. acknowledges the American University of Sharjah for Faculty Research Grant (FRG12-2-14).

Notes and references

1 (*a*) P. Kaur, J. T. Hupp and S. B. T. Nguyen, *ACS Catal.*, 2011, **1**, 819; (*b*) Y. Zhang and S. N. Riduan, *Chem. Soc. Rev.*, 2012, **41**, 2083.
2 (*a*) N. A. Rakow, M. S. Wendland, J. E. Trend, R. J. Poirier, D. M. Paolucci, S. P. Maki, C. S. Lyons and M. J. Swierczek, *Langmuir*, 2010, **26**, 3767; (*b*) X. Liu, Y. Xu and D. Jiang, *J. Am. Chem. Soc.*, 2012, **134**, 8738.
3 (*a*) R. Dawson, A. I. Cooper and D. J. Adams, *Prog. Polym. Sci.*, 2012, **37**, 530; (*b*) R. Dawson, E. Stockel, J. R. Holst, D. J. Adams and A. I. Cooper, *Energy Environ. Sci.*, 2011, **4**, 4239; (*c*) T. C. Drage, C. E. Snape, L. A. Stevens, J. Wood, J. Wang, A. I. Cooper, R. Dawson, X. Guo, C. Satterley and R. Irons, *J. Mater. Chem.*, 2012, **22**, 2815.
4 (*a*) D. Yuan, W. Lu, D. Zhao and H.-C. Zhou, *Adv. Mater.*, 2011, **23**, 3723; (*b*) W. Lu, D. Yuan, J. Sculley, D. Zhao, R. Krishna and H.-C. Zhou, *J. Am. Chem. Soc.*, 2011, **133**, 18126; (*c*) W. Lu, J. P. Sculley, D. Yuan, R. Krishna, Z. Wei and H.-C. Zhou, *Angew. Chem., Int. Ed.*, 2012, **51**, 7480.
5 M. G. Rabbani and H. M. El-Kaderi, *Chem. Mater.*, 2012, **24**, 1511.
6 M. G. Rabbani and H. M. El-Kaderi, *Chem. Mater.*, 2011, **23**, 1650.
7 M. G. Rabbani, T. E. Reich, R. M. Kassab, K. T. Jackson and H. M. El-Kaderi, *Chem. Commun.*, 2012, **48**, 1141.
8 K. Sumida, D. L. Rogow, J. A. Mason, T. M. McDonald, E. D. Bloch, Z. R. Herm, T.-H. Bae and J. R. Long, *Chem. Rev.*, 2012, **112**, 724.
9 (*a*) G. T. Rochelle, *Science*, 2009, **325**, 1652; (*b*) D. M. D'Alessandro, B. Smit and J. R. Long, *Angew. Chem., Int. Ed.*, 2010, **49**, 6058.
10 (*a*) Y.-S. Bae and R. Q. Snurr, *Angew. Chem., Int. Ed.*, 2011, **50**, 11586; (*b*) J.-R. Li, J. Sculley and H.-C. Zhou, *Chem. Rev.*, 2012, **112**, 869.
11 Annual Energy Outlook, 2012 (AEO2012) Early Release Overview. (http://www.eia.gov/forecasts/aeo/er/pdf/0383er(2012).pdf).
12 G. Venkataramana and S. Sankararaman, *Eur. J. Org. Chem.*, 2005, **19**, 4162.
13 (*a*) E. W. Neuse and M. S. Loonat, *Macromolecules*, 1983, **16**, 128; (*b*) S. Lin and L. Yang, *Tetrahedron Lett.*, 2005, **46**, 4315.
14 P. Totsatitpaisan, S. P. Nunes, K. Tashiro and S. Chirachanchai, *Solid State Ionics*, 2009, **180**, 738.
15 Q. Chen, M. Luo, P. Hammershøj, D. Zhou, Y. Han, B. W. Laursen, C.-G. Yan and B.-H. Han, *J. Am. Chem. Soc.*, 2012, **134**, 6084.
16 A. P. Katsoulidis and M. G. Kanatzidis, *Chem. Mater.*, 2011, **23**, 1818.
17 S. Keskin, T. M. van Heest and D. S. Sholl, *ChemSusChem*, 2010, **3**, 879.
18 H. Furukawa and O. M. Yaghi, *J. Am. Chem. Soc.*, 2009, **131**, 8875.
19 R. Dawson, D. J. Adams and A. I. Cooper, *Chem. Sci.*, 2011, **2**, 1173.
20 (*a*) X.-J. Zhang, N. Bian, L.-J. Mao, Q. Chen, L. Fang, A.-D. Qi and B.-H. Han, *Macromol. Chem. Phys.*, 2012, **213**, 1575; (*b*) Y.-C. Zhao, Q.-Y. Cheng, D. Zhou, T. Wang and B.-H. Han, *J. Mater. Chem.*, 2012, **22**, 11509.
21 M. Mastalerz, M. W. Schneider, I. M. Oppel and O. Presly, *Angew. Chem., Int. Ed.*, 2011, **50**, 1046.
22 H. Kim, Y. Kim, M. Yoon, S. Lim, S. M. Park, G. Seo and K. Kim, *J. Am. Chem. Soc.*, 2010, **132**, 12200.
23 (*a*) A. Phan, C. J. Doonan, F. J. Uriberomo, C. B. Knobler, M. O'Keeffe and O. M. Yaghi, *Acc. Chem. Res.*, 2010, **43**, 58; (*b*) R. Banerjee, H. Furukawa, D. Britt, C. Knobler, M. O'Keeffe and O. M. Yaghi, *J. Am. Chem. Soc.*, 2009, **131**, 3875.
24 J. L. C. Rowsell and O. M. Yaghi, *J. Am. Chem. Soc.*, 2006, **128**, 1304.
25 P. Huanhua, J. A. Ritter and P. B. Balbuena, *Langmuir*, 1998, **14**, 6323.
26 S. Tedds, A. Walton, D. P. Broom and D. Book, *Faraday Discuss.*, 2011, **151**, 75.
27 P. Mohanty, L. D. Kull and K. Landskron, *Nat. Commun.*, 2011, DOI: 10.1038/ncomms1405.
28 A. Laybourn, R. Dawson, R. Clowes, J. A. Iggo, A. I. Cooper, Y. Z. Khimyak and D. J. Adams, *Polym. Chem.*, 2012, **3**, 533.
29 (*a*) A. Samanta, A. Zhao, G. K. H. Shimizu, P. Sarkar and R. Gupta, *Ind. Eng. Chem. Res.*, 2012, **51**, 1438; (*b*) J. An, S. J. Geib and N. L. Rosi, *J. Am. Chem. Soc.*, 2010, **132**, 38; (*c*) A. Demessence, D. M. D'Alessandro, M. L. Foo and J. R. Long, *J. Am. Chem. Soc.*, 2009, **131**, 8784; (*d*) R. Vaidhyanathan, S. S. Iremonger, K. W. Dawson and G. H. K. Shimizu, *Chem. Commun.*, 2009, 5230.
30 (*a*) T. Panda, P. Pachfule, Y. Chen, J. Jiangb and R. Banerjee, *Chem. Commun.*, 2011, **47**, 2011; (*b*) B. Zheng, J. Bai, J. Duan, L. Wojtas and M. J. Zaworotko, *J. Am. Chem. Soc.*, 2011, **133**, 748.
31 R. Vaidhyanathan, S. S. Iremonger, G. H. K. Shimizu, P. G. Boyd, S. Alavi and T. K. Woo, *Science*, 2010, **330**, 650.
32 D.-S. Zhang, Z. Chang, Y.-B. Lv, T.-L. Hu and X.-H. Bu, *RSC Adv.*, 2012, **2**, 408.
33 (*a*) D. L. Greene, J. R. Kahn and R. C. Gibson, *Energy*, 1999, **20**, 1; (*b*) A. Zuttel, *Mater. Today*, 2003, **6**, 24; (*c*) L. Schlapbach and A. Zuttel, *Nature*, 2001, **414**, 353.
34 (*a*) B. S. Ghanem, M. Hashem, K. D. M. Harris, K. J. Msayib, M. Xu, P. M. Budd, N. Chaukura, D. Book, S. Tedds, A. Walton and N. B. McKeown, *Macromolecules*, 2010, **43**, 5287; (*b*) A. Thomas, P. Kuhn, J. Weber, M.-M. Titirici and M. Antonietti, *Macromol. Rapid Commun.*, 2009, **30**, 221; (*c*) C. D. Wood, B. Tan, A. Trewin, H. Niu, D. Bradshaw, M. J. Rosseinsky, Y. Z. Khimyak, N. L. Campbell, R. Stöckel, E. Kirk and A. I. Cooper, *Chem. Mater.*, 2007, **19**, 2034.
35 Z. Wang, B. Zhang, H. Yu, L. Sun, C. Jiaob and W. Liua, *Chem. Commun.*, 2010, **46**, 7730.
36 (*a*) T. Ben, H. Ren, S. Q. Ma, D. P. Cao, J. H. Lan, X. F. Jing, W. C. Wang, J. Xu, F. Deng, J. M. Simmons, S. L. Qiu and G. S. Zhu, *Angew. Chem., Int. Ed.*, 2009, **48**, 9457; (*b*) T. Ben, C. Pei, D. Zhang, J. Xu, F. Deng, X. Jing and S. Qiu, *Energy Environ. Sci.*, 2011, **4**, 3991.
37 W. Lu, D. Yuan, D. Zhao, C. I. Schilling, O. Plietzsch, T. Muller, S. Bräse, J. Guenther, J. Blümel, R. Krishna, Z. Li and H.-C. Zhou, *Chem. Mater.*, 2010, **22**, 5964.
38 J. Lewiński, T. Kaczorowski, D. Prochowicz, T. Lipińska, I. Justyniak, Z. Kaszkur and J. Lipkowski, *Angew. Chem., Int. Ed.*, 2010, **49**, 7035.
39 (*a*) Y. Jin, B. A. Voss, A. Jin, H. Long, R. D. Noble and W. Zhang, *J. Am. Chem. Soc.*, 2011, **133**, 6650; (*b*) Y. Jin, B. A. Voss, R. McCaffrey, C. T. Baggett, R. D. Noble and W. Zhang, *Chem. Sci.*, 2012, **3**, 874.
40 (*a*) O. K. Farha, A. Spokoyny, B. Hauser, Y.-S. Bae, S. Brown, R. Q. Snurr, C. A. Mirkin and J. T. Hupp, *Chem. Mater.*, 2009, **21**, 3033; (*b*) O. K. Farha, Y.-S. Bae, B. G. Hauser, A. M. Spokoyny, R. Q. Snurr, C. A. Mirkin and J. T. Hupp, *Chem. Commun.*, 2010, **46**, 1056.
41 J.-R. Li, Y. Ma, M. C. McCarthy, J. Sculley, J. Yu, H.-K. Jeong, P. B. Balbuena and H.-C. Zhou, *Coord. Chem. Rev.*, 2011, **255**, 1791.
42 T. Burchell and M. Rogers, *SAE Tech. Pap. Ser.*, 2000, 2001.
43 U. S. Department of Energy, *Energy Efficiency and Renewable Energy*, http://www1.eere.energy.gov/hydrogenandfuelcells/mypp/pdfs/storage.pdf, accessed 10 September, 2012.
44 C. F. Martin, E. Stöckel, R. Clowes, D. J. Adams, A. I. Cooper, J. J. Pis, F. Rubiera and C. Pevida, *J. Mater. Chem.*, 2011, **21**, 5475.
45 M. P. Suh, H. J. Park, T. K. Prasad and D. W. Lim, *Chem. Rev.*, 2012, **112**, 782.
46 A. L. Myers and J. M. Prausnitz, *AIChE J.*, 1965, **11**, 121.

47 (*a*) Z. R. Herm, J. A. Swisher, B. Smit, R. Krishna and J. R. Long, *J. Am. Chem. Soc.*, 2011, **133**, 5664; (*b*) Y.-S. Bae, O. K. Farha, J. T. Hupp and R. Q. Snurr, *J. Mater. Chem.*, 2009, **19**, 2131.
48 F. Akhtar, Q. Liu, N. Hedin and L. Bergström, *Energy Environ. Sci.*, 2012, **5**, 7664.
49 R. T. Yang, *Adsorbents: Fundamentals and Applications*, John Wiley & Sons, Inc., Hoboken, 2003.